Journal of Marine Systems 211 (2020) 103414

Contents lists available at ScienceDirect

Journal of Marine Systems

journal homepage: www.elsevier.com/locate/jmarsys

New production across the shelf-edge in the northeastern North Sea during the stratified summer period

Jørgen Bendtsen[a,*], Katherine Richardson[b]

[a] Norwegian Institute for Water Research, NIVA Denmark, 2300 Copenhagen S, Denmark
[b] Center for Macroecology, Evolution and Climate, Globe Institute, University of Copenhagen, 2100 Copenhagen O, Denmark

ARTICLE INFO

Keywords:
New production
Nitrate assimilation
Biological pump
Shelf edge
Regional modelling
North Sea

ABSTRACT

New production of organic matter from photosynthesis based on "new" nitrate transported into the illuminated surface layer fuels temperate ecosystems during periods of stratification when surface waters are nutrient limited. Published observations from the northeastern North Sea show a large spatial heterogeneity in vertical nitrate fluxes and suggest shelf edge mixing may be the major source for new production here during the stratified summer season. In the current study, we further investigate these empirical findings with a numerical model, where physical transports and mixing are evaluated against observations of temperature, salinity, nutrients and dissipation of turbulent kinetic energy. The relatively shallow central North Sea is separated from the deep Norwegian trench by a strong shelf edge current. This shelf edge frontal zone is characterized by a vertical separation of the surface and benthic boundary layers by an intermediate layer exhibiting low turbulence. A new nitrate assimilation model, driven by light and nitrate availability, is developed and applied for quantifying the potential for, and distribution of, new production in the area. New production in the frontal zone above the shelf edge is located in a narrow high productive ($\sim$100 mg C m^{-2} day^{-1}) band. This is in qualitative accordance with observations. The model results also suggest, however, that new production of similar magnitude occurs above the deep Norwegian trench, where a shallow nutricline in combination with mesoscale eddy activity leads to increased transport of nitrate to the surface layer. Increased new production along the shelf edge could potentially impact ecosystem structure and may explain the relatively high species richness and fishing activity recorded in this part of the North Sea.

1. Introduction

Primary production in the ocean is understood as being comprised of two forms. Dugdale and Goering (1967) designated these as *new* and *regenerated* production, where the former is driven by an allochthonous nutrient (nitrogen) source and the latter by a nitrogen source that has been regenerated (through heterotrophic processes) locally, i.e., within the system, itself. The differentiation between these two forms is important as it is only new production that can lead to a net increase in the production of organic material. Thus, the percentage of new production with respect to total primary production (designated *f-ratio* by Eppley and Peterson, 1979) is a critical determinant of food availability for marine food webs and for the amount of organic material that can sink from surface to deep water ocean layers (*biological pump*; Volk and Hoffert, 1985).

From direct in situ determination of *f-ratios* (using ^{15}N isotopes, e.g. Dugdale and Wilkerson, 1986), it is known that the *f-ratio* varies in time and space, both geographically and through the water column. Estimates of total primary production (both in situ estimates based on ^{14}C incorporation and estimates based on optical characteristics of the surface ocean) cannot differentiate between new and regenerated production. Thus, estimates of total primary production are difficult to directly relate to the net production of new organic material. In other words, two regions where total primary production estimates are similar can have vastly different potential for supporting productive food webs and/or contributing to export of organic material from surface to deep waters.

For seasonally stratified coastal shelf regions, the general assumption has been that new production and, thereby, the *f-ratio* is high during the spring bloom, when the nutrients found in surface waters originate from winter mixing and can, therefore, be considered as allochthonous. On the other hand, it has been assumed that the *f-ratio* will be low during summer months when water column stratification hinders the transfer of nutrients from deep to surface waters.

* Corresponding author.
E-mail address: jb@niva-dk.dk (J. Bendtsen).

https://doi.org/10.1016/j.jmarsys.2020.103414
Received 28 April 2020; Received in revised form 8 July 2020; Accepted 13 July 2020
Available online 18 July 2020

Numerous studies, however, have given cause to reconsider the assumption of low new production in seasonally stratified shelf seas during summer months, i.e. the period of stratification. Direct determination of *f-ratios* over larger geographic regions is not feasible but *f-ratios* can also be estimated from vertical nutrient fluxes, i.e., estimates of the delivery of allochthonous nutrients (nitrogen) input to the illuminated surface waters where photosynthesis takes place. Through a combination of direct measurement and nutrient flux estimates, a number of studies have identified local "hot spots" with elevated f-ratios during summer months in coastal shelf waters around the world.

Often, these "hotspots" are associated with a subsurface chlorophyll maxima (SCM) and are, therefore, not observable from data collected in surface waters. In a study of the Celtic Sea, for example, Hickman et al. (2012) estimated that the magnitude of new production occurring in association with the SCM could be about half of that occurring in the spring bloom. In an observational study including measurements of turbulence and nitrate, Sharples et al. (2001) suggested that transport of nutrients from deep waters to the SCM could support a new production in the Western English Channel on the order of 160 mg C m^{-2} day^{-1} and be a potentially important source of material exported from surface to deep waters. For the North Sea, Richardson and Pedersen (1998) estimated that ~20% of annual new production could potentially be supported by the tidal mixing of nutrient rich deep waters to an intermediate depth layer supporting the SCM. In addition, Weston et al. (2005) estimated that ~37% of the annual new production occurring in the central North Sea might be associated with the SCM.

Thus, there is considerable evidence that there is a potential for new production to occur below the surface ocean layer in and around the North Sea during the period of seasonal stratification. A weakness in many of these studies, however, is that they are based on upscaling of measurements made over very limited geographical areas. We (Bendtsen and Richardson, 2018; hereafter BR2018) have earlier reported on a field study where turbulence measurements were collected throughout the water column over a large region of the northeastern North Sea. We used these to estimate the vertical flux of nitrate from deep to surface waters and estimated the potential for new production from these fluxes. That study suggested considerable heterogeneity in the distribution of new production in this region, where high values were located at sites located along the shelf edge and at a locality near the Norwegian coast.

In the current study, we further explore the potential for new production in this region during the summer stratified period by developing a nitrate assimilation (representing new production) model which is driven by light and nitrate availability in an attempt to quantify the potential for, and distribution of, new production over this entire region. The model results suggest that new production takes place in sub-surface waters along the shelf edge and, in addition, that new production is associated with eddy activity occurring in the deeper area off the shelf edge.

2. Methods

2.1. Model description

The ocean model used to represent North Sea characteristics is based on the COHERENS circulation model (Luyten, 2014). COHERENS solves the primitive equations, i.e. momentum equations with the Boussinesq approximation, mass and energy conservation and applies a non-linear equation of state. The model domain covers the entire North and Baltic Seas (Fig. 1a) and is formulated on an equidistant spherical grid with a horizontal resolution of ~2 × 2 nautical miles and 20 stretched vertical sigma-layers (Song and Haidvogel, 1994) in the deeper areas (> 50 m) with a smooth transition to equidistant layer thickness in the shallow areas (Siddorn and Furner, 2013).

The baroclinic pressure gradient is discretized by the cubic-H

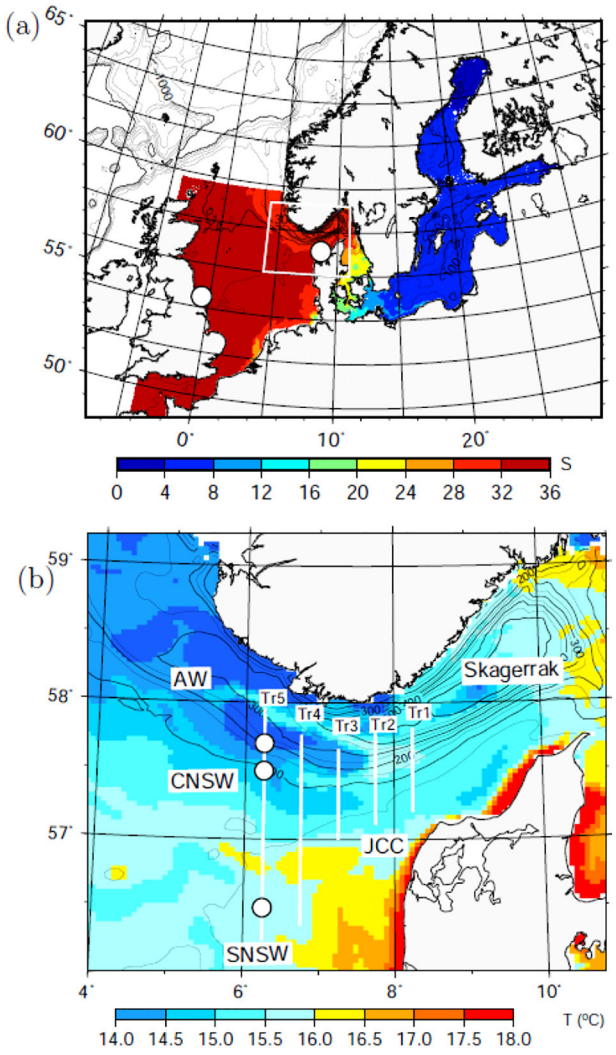

Fig. 1. (a) Model domain and (b) study area showing VERMIX transect 1–5 (BR2018) and three locations along transect 5 (circles) analyzed in Fig. 7. Colors show (a) salinity and (b) temperature (19 July 2016). In (a) bathymetry outside the model domain is contoured in intervals of 500 m above 1000 m depth and 200 m intervals below. Tide gauge stations in Whitby and Hanstholm are shown (white bullets) and the rectangle in (a) shows the area in (b).

method (Shchepetkin and McWilliams, 2003) and advective transports are determined by a TVD-scheme. Vertical mixing is described by a k-ε turbulent model with a background viscosity and diffusion coefficient of $0.1{\cdot}10^{-5}$ m^2 s^{-1} and, due to the relatively high horizontal resolution, there is no explicit horizontal turbulent viscosity and diffusivity. The model equations are solved by a multigrid method with a barotropic and baroclinic time step of 50 and 5 s, respectively.

The model is confined within boundaries at 48°N and 3.85°W in the North Sea, i.e. between the Shetland Islands and Norway and in the English Channel (Fig. 1a), and the model bathymetry is interpolated from the high-resolution (⅛ x ⅛ degree) EMODnet bathymetry (EMODnet Bathymetry Consortium, 2016). The bathymetry in the North Sea/Baltic Sea transition zone is modified to take into account the relatively deep and narrow straits in the Great Belt and The Sound (Bendtsen et al., 2009). The minimum depth is 10 m in the North Sea and 5 m in the Baltic Sea and a low-pass filter reduces bottom-slope to less than 0.18 in the model domain.

Tidal forcing is described by sea level and volume transports across the open boundaries from the eight most significant tidal constituents extracted from the barotropic OTIS North Sea model of Egbert and Erofeeva (2002). The model includes the 50 largest rivers in the North

Sea and the Baltic Sea area and runoff is based on monthly climatological values. Meteorological forcing is based on ERA5 (dataset obtained from Copernicus Climate Change Service, 2017) where wind, air temperature, cloudiness, relative humidity, precipitation, air pressure and sea ice distribution are interpolated onto the model grid in 3-hour intervals. Surface fluxes are reduced proportionally to sea ice cover.

2.2. Initial conditions and open boundary conditions

The model is initialized with temperature and salinity distributions on 1 January 2016. The first two months are considered as model spin up where temperature, salinity and water level equilibrate with the model forcing. Tidal motion in the model was found to equilibrate within a few weeks and we, therefore, assume that a two-month spin up period is sufficient for resolving the general dynamics and water mass distributions in the northeastern North Sea (note, however, that a much longer spin up would be required for equilibrating the entire North Sea/Baltic Sea system with respect to the salinity and temperature differences across the North Sea/Baltic Sea transition zone). The initial fields applied in the model are provided from high resolution operational models, and the dynamics in the study region are expected mainly to be influenced by out- and inflow to the Skagerrak region. A characteristic quasi-stationary current pattern was established along the shelf edge after the two month spin up period.

2.2.1. Temperature and salinity

Initial conditions of temperature and salinity are based on re-analyzed temperature and salinity fields obtained from the Copernicus Marine Data server (CMEMS). The Initial field for the North Sea is based on the FOAM AMM7 (Forecasting Ocean Assimilation Model, 7 km resolution Atlantic Margin Model; O'Dea et al., 2012) re-analyzed fields (CMEMS, northwestshelf_reanalysis_phy_004_009) of the North West European Shelf. Fields from the Baltic Sea are obtained from the NEMO-Nordic re-analysis (CMEMS, balticsea_reanalysis_phy_003_011; Hordoir et al., 2019). It should be noted that the use of output from two different models for creating initial conditions is consistent because the open boundaries towards the Baltic of the FOAM AMM7 model are determined by output from the NEMO-Nordic model. The two datasets are merged to obtain initial fields for the entire model domain on 1 January 2016.

Open boundary conditions in the North Sea towards the north Atlantic and the English Channel were generated from monthly averages of the FOAM AMM7 daily averaged fields of currents, temperature and salinity in 2016. Volume transports at the open boundaries were determined by a radiation condition (derived by the method of characteristics) and fluxes of temperature and salinity were calculated from the climatological fields.

2.2.2. Nitrate

Nitrate was applied in the idealized nitrate-assimilation model experiment for a two-month period and it was initialized from 1 June. The first month was considered as a spin up period where nitrate equilibrated with the dynamics and biological nitrate-assimilation in the northeastern North Sea.

It was assumed that the initial field of nitrate could be represented by monthly climatological values in June. The focus of this study is on conditions in the northeastern North Sea and, therefore, it was also assumed that only nitrate distributions in this part of the North Sea had a significant influence on conditions in the shelf edge area. Thus, nitrate sources associated with runoff (e.g., in the German Bight), inflow from the English Channel or conditions in the Baltic Sea were not considered to be critical for nitrate assimilation along the shelf edge during the study period.

An initial field of nitrate in June was created from the monthly North Sea Biogeochemical Climatology of Hinrichs et al. (2017). This relatively high-resolution data-set (horizontal resolution of ¼ x ¼ degrees), covering the entire North Sea and the western Baltic Sea, was merged with the World Ocean Atlas 2018 climatology (Garcia et al., 2018; horizontal resolution of 1 × 1 degrees) for the remaining Baltic Sea area. The initial nitrate field in the Baltic Sea was assumed to be unimportant for the conditions in the northeastern North Sea during the model experiment.

Open boundary conditions were obtained from the climatological nitrate values in June along the northern boundary and were held constant during the two-month period. A no-flux condition was applied for transports through the western boundaries, i.e. the English Channel and between the Scotland and Shetland Islands.

2.3. Model validation

The model was analyzed from March–October 2016 and the model results were qualitatively compared with observations of sea level from tide gauges, and fields of temperature, salinity and dissipation of turbulent kinetic energy obtained in July on the VERMIX cruise. The comparison provided information on the general model performance on simulating tides, i.e. a major energy source for mixing in the area, and the ability to simulate the general distribution of water masses and turbulence in the shelf edge region in the northeastern North Sea.

2.3.1. Tide gauge data

Tide gauge data were obtained from the Copernicus Data Store and were used for evaluating the model's simulation of tides. The model was evaluated from 28 tide gauge stations covering the entire model domain. In general, there was a good agreement between simulated and observed water level changes and two examples from each side of the North Sea were considered in more detail (Fig. S1): Tidal forcing at the western side of the North Sea (Whitby, UK) resulted in a relatively large tidal amplitude (~2 m) and there was a good accordance between the model and observations. The weaker tidal amplitude (< 0.5 m) on the eastern coast of the North Sea (Hanstholm, DK) was also well simulated by the model (i.e., phase and amplitude). However, the eastern side is relatively more influenced by wind forcing than the western side (due to the smaller amplitude) and small deviations between the model simulations and observations due to short-term “surge-events” were seen at Hanstholm (e.g., 4–7 July in Fig. S1b). These deviations may be explained by the simplified open boundary conditions (using monthly averaged conditions) or due to limitations associated with the meteorological forcing fields. Thus, we consider the tides to be well described by the model, and the relatively small model deviations compared to the tidal range during short periods along the eastern North Sea coast do not impact the conclusions of this study.

2.3.2. VERMIX observations in July 2016

The observations obtained on the VERMIX cruise in July 2016 (described in BR2018) are used for evaluating the model simulation in the stratified summer period. The VERMIX cruise, covering the northeastern North Sea from the shallow shelf and across the Norwegian trench towards Norway, included measurements of temperature and salinity (made with a Seabird 911+ system; salinity is reported as practical salinity). In addition, dissipation rates of turbulent kinetic energy (TKE) were calculated from observed microstructure of current shear (made with a Rockland Scientific International VMP-250 microstructure vertical profiler) along five transects (shown in Fig. 1b). The water mass distributions and microstructure observations across the shelf edge were found to be qualitatively similar along the five transects, as is further described in BR2018. Therefore, distributions along one transect (5) are applied for the model evaluation in this study (Fig. 2). The observations showed the presence of Southern and Central North Sea water (SNSW, S = 34.50–34.80; CNSW, S = 34.80–35.00, both water masses in the temperature range between 8 and 10 °C) above the more shallow part of the shelf-edge region at a depth of ~60 m (~56.88°N in Fig. 2). High-saline Atlantic water masses were

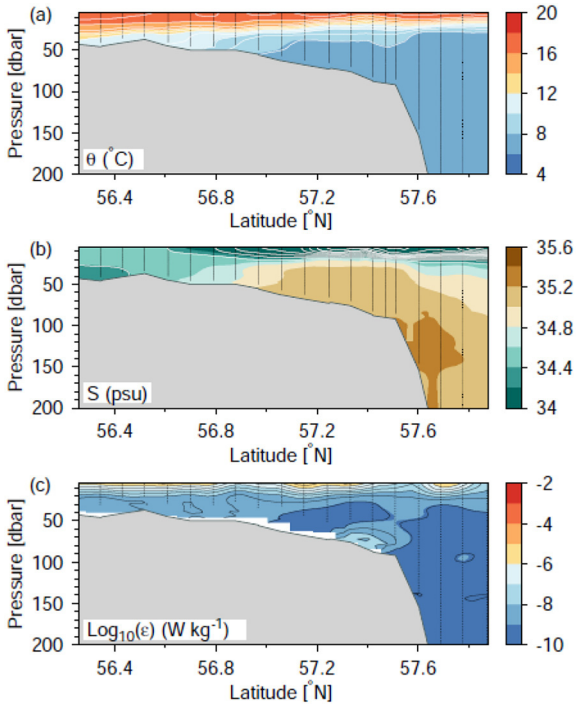

Fig. 2. VERMIX observations of (a) potential temperature, (b) salinity and (c) dissipation rate of TKE along transect 5 (6.25°E, 56.25–59.9°N) measured between 24 and 26 July 2016. Note that the bottom boundary layer is not resolved from observations in (c).

located at the shelf edge (S > 35.00) with a core of high-saline deep Atlantic water (S = 35.15–35.32, T = 7–10 °C) below ~80 m depth and low-saline recirculated Skagerrak water dominated the upper water masses towards the Norwegian coast.

Nutrients were, in general, depleted in the surface layer during the VERMIX cruise and, in the southern part of the transects, i.e. above the shallow shelf, the entire water column was found to be nitrate-depleted whereas high nitrate concentrations were observed in the high-saline Atlantic water masses along the shelf-edge and above the Norwegian trench (Fig. 3). This characteristic nutrient field during the summer season is also apparent in climatological fields from the area (Fig. S2) and it motivated the simple model experiment where nitrate was initialized in June.

2.4. Nitrate assimilation model

Primary production (PP) is calculated from chlorophyll *a* (*chl*), photosynthetic available radiation (PAR) and nutrients. Nitrate is assumed to be the limiting nutrient during the stratified period in the area, supported by the observed nitrate depletion in the surface layer (Fig. 3). In general, PP can be calculated from the photosynthetic parameters ($P_{max}{}^B$, α^B, β^B), *chl* and PAR (Platt et al., 1980) and here we also included access to nutrients:

$$\mathrm{PP} = P^B_{max}\,chl\left(1-\exp\left(-\mathrm{PAR}\frac{\alpha^B}{P^B_{max}}\right)\right)\exp\left(-\mathrm{PAR}\frac{\beta^B}{P^B_{max}}\right)\lambda_N \quad (1)$$

where PAR, photosynthetic parameters and chlorophyll *a*, in general, vary through the water column. Phytoplankton also requires access to nutrients and this is included by the nitrate limitation term (λ_N).

Here, we assume that the photosynthetic parameters and chlorophyll *a* can be represented by constant values in the euphotic zone, calculated from the average of observed values from the VERMIX cruise in the surface layer and in the SCM. The parameters vary by about a factor of two between the surface and the SCM in the area (Table 1). Thus, the vertical variation in PP due to adaptation of the phytoplankton community to changes in the light field is not resolved in detail by the model. As photosynthetic parameters have been found to vary significantly both temporally and spatially (Richardson et al., 2016), we, nevertheless, consider the averaged values from the area to be representative of the water column as a whole.

The assumption of a constant chlorophyll *a* concentration in the euphotic zone represents a more critical assumption as this simplification disregards the vertical gradient from low surface values towards the SCM. The implications of this assumption were considered in a sensitivity study (see below).

Nitrate (N) is assumed to be the limiting nutrient, thus nutrient limitation of PP is parameterized according to the following Monod equation:

$$\lambda_N = \frac{\mathrm{N}}{\mathrm{N}+\kappa} \quad (2)$$

where the half saturation constant (κ) has the relatively low value of 0.01 mmol N m^{-3} (Richardson and Bendtsen, 2017).

Nitrate assimilation (NA) is assumed to be related to PP via a constant Redfield N:C molar ratio ($\eta_{N:C}$) of 16:106 (Redfield et al., 1963) and is determined from:

$$\mathrm{NA}(\mathrm{N},\mathrm{PAR}) = -\eta_{N:C}\mathrm{PP} \quad (3)$$

Thus, NA depends on the varying N and PAR distributions.

Nitrate is included in the circulation model and the spatial and temporal distributions of N are determined from the transport equation where NA is included as a local nitrate sink. The PAR distribution is calculated from the incoming irradiance at the surface (depending on time, location and cloudiness and updated every hour) and a constant light attenuation coefficient of 0.14 m^{-1}, which was found to

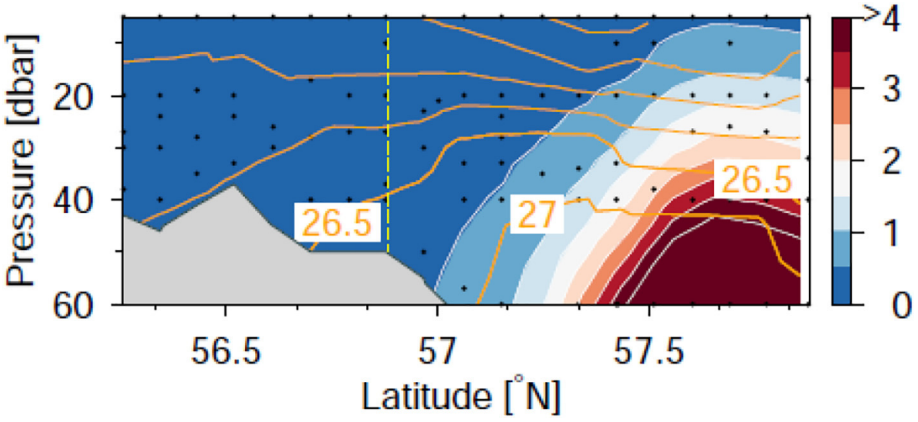

Fig. 3. (a) VERMIX observations of nitrate (colors) and contours of potential density anomalies (in intervals of 0.5 kg m^{-3}) along transect 5.

Table 1
Model parameters. Average values from the VERMIX cruise (BR2018) applied in the nitrate assimilation model.

Parameter	Observed surface (5 m)	Observed SCM (~27 m)	Average value	Unit	Description
chl	0.16	1.67	0.92	[mg chl m^{-3}]	Chlorophyll *a*
P^B_{max}	5.48	2.33	3.91	[μg C (μg chl h)$^{-1}$]	Photosynthetic parameters
α^B	4.10	2.70	3.4	10^{-2}·[μg C(μg chl h μE m^{-2} s^{-1})$^{-1}$]	
β^B	1.70	3.00	2.35	10^{-3}·[μg C (μg chl h μE m^{-2} s^{-1})$^{-1}$]	

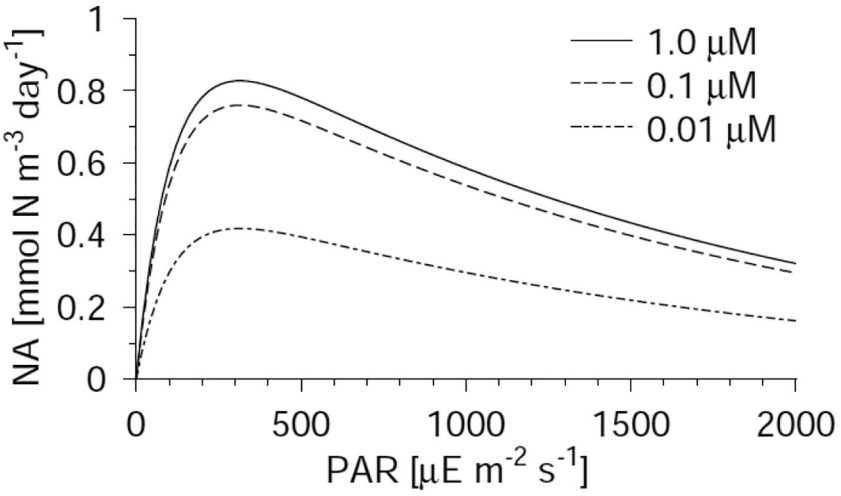

Fig. 4. Nitrate assimilation as a function of PAR for different nitrate concentrations (Eq. 3).

characterize the conditions in the area (BR2018).

The NA was calculated for various nutrient and light conditions (Fig. 4). It has the shape of a typical PP vs PAR curve (e.g. BR2018) with a maximum at ~300 μE m^{-2} s^{-1} and a decrease at higher light levels due to photoinhibition (i.e. described by β^B). The maximum nitrate assimilation for a concentration of 1 mmol N m^{-3} is ~0.8 mmol N m^{-3} day^{-1}, corresponding to 64 mg C m^{-3} day^{-1}.

Nitrate is the only nutrient source for PP in the model experiment. Furthermore, regenerated production from re-mineralized organic matter is not included. Therefore, PP becomes equivalent to new production (NP). Thus, NP is calculated from the vertically integrated nitrate assimilation in the euphotic zone (Z_{eup}):

$$\mathrm{NP} = \frac{1}{\eta_{N:C}} \int_{Z_{eup}}^{0} \mathrm{NA}(\mathrm{N}, \mathrm{PAR})\, dz \tag{4}$$

The euphotic zone was defined between the surface and the depth where PAR reached 0.1% of its surface value, i.e. $Z_{eup} \sim -50$ m.

To identify the spatial distribution of new production across the shelf edge, the locally accumulated nitrate assimilation (*AcNA*) was defined as:

$$AcNA = \int \mathrm{NA}(\mathrm{N}, \mathrm{PAR})\, dt \tag{5}$$

3. Results

Physical conditions and nitrate assimilation were analyzed along the five transects in the northeastern North Sea occupied during the VERMIX study. The five transects cover a region above the deep Norwegian trench, where Atlantic water masses gradually mix with less saline water from the Baltic Sea and the southern North Sea.

The averaged pattern of water mass distributions in July 2016 (Fig. 5) was characterized by inflowing (eastward) Atlantic water centered above the shelf edge and recirculating outflowing water located in the region stretching from above the deep Norwegian trench and towards the Norwegian coast. The region associated with the meeting of the currents of opposing directions (i.e., the in- and out-flowing currents) was associated with a large horizontal density gradient (see Fig. 5, where the 27 kg m^{-3} pycnostad is located at the separation of the currents). Model fields of temperature and salinity were found to be in general accordance with observations along transect 5 in the BR2018 study (Fig. 2).

3.1. Turbulence across the shelf edge

The simulated dissipation rates of TKE were analyzed along a section corresponding to transect 5 in the BR2018 study. The monthly averaged field showed a separation between the surface and benthic bottom layer above the shallow shelf (Fig. 6a). The two layers were separated by a 10–20 m thick intermediate layer with dissipation rates below 10^{-7} W kg^{-1}. Above the deep Norwegian trench and below the surface layer, dissipation rates were $< 10^{-8}$ W kg^{-1}. The transition from this low-turbulent regime to the shallow shelf was seen at a bottom depth of ~80 m at the shelf edge. The conditions near the Norwegian coast have minor influence on the turbulence field in the northern part of the transect because of the relatively steep bottom topography there. Observations of dissipation rates of TKE along transect 5 were obtained in calm weather between 24 and 26 July (Fig. 2c) and model results were averaged for the same period (Fig. 6b). The model simulation also revealed a low turbulent regime below the surface layer above the Norwegian trench ($< 10^{-9}$ W kg^{-1}) and relatively low dissipation rates above the shallow area (compared with the monthly averaged values). These distributions were in accordance with observations. Higher dissipation rates (~10^{-8} W kg^{-1}) were simulated above the shelf edge which was also in accordance with the distributions obtained on the field study for the same bottom depth range (~80 m). Observations resolved only conditions above the benthic boundary layer along transect 5. However, the bottom boundary layer was resolved on other transects (shown in BR2018) and found to be in qualitative accordance with the model simulation.

The corresponding distribution of the vertical turbulent diffusion coefficient above the shallow North Sea and towards the shelf edge showed a similar intermediate layer with relatively low values, i.e.,

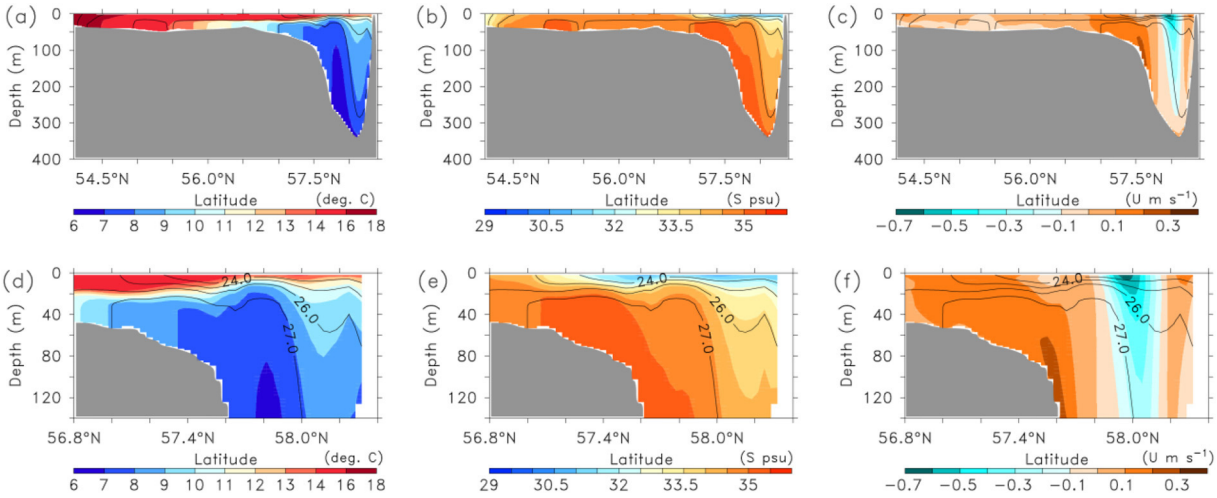

Fig. 5. Simulated water mass distributions across the shelf edge. Average conditions for July 2016 of (a, d) potential temperature (°C), (b, e) salinity (psu) and (c, f) eastward current (m s^{-1}) along transect 5 (6.25°E). The lower figures show a zoom of the shelf edge conditions. A relatively warm water column characterized the southern part of the transect ($T > 16$ °C, S ~ 33) and stratification increased towards the shelf edge. An eastward current with velocities > 0.2 m s^{-1} was centered above the shelf edge (bottom depth ~100 m) and westward flowing water masses located above the Norwegian trench showed current speeds > 0.3 m s^{-1} in the upper 100 m.

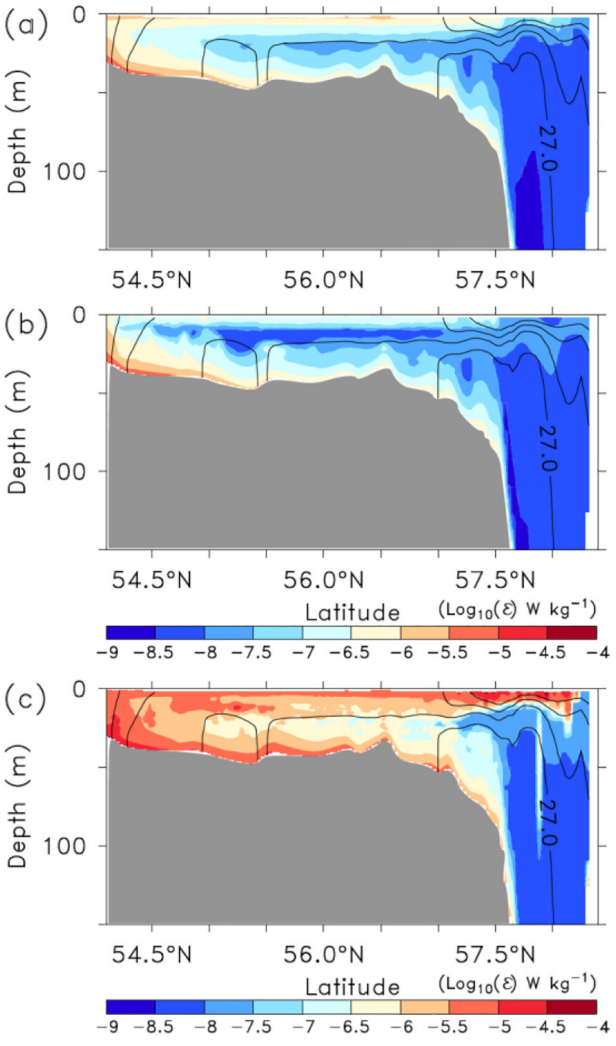

Fig. 6. Simulated distribution of dissipation rate of TKE in July 2016 ($Log_{10}(\varepsilon)$, W kg^{-1}) along transect 5. (a) The monthly averaged field in July, (b) the average between 24 and 26 July and (c) the maximum value in July. Contours of potential density anomalies are shown in intervals of 0.5 kg m^{-3}.

10^{-5}–10^{-6} m^2 s^{-1}, in the depth range ~10–30 m surrounded by higher values in the surface and bottom boundary layers (Fig. S3). This was in qualitative accordance with estimated vertical diffusion coefficients across the shelf edge (Fig. 6 in BR2018) where minimum values of ~10^{-6} m^2 s^{-1} were located at 20–40 m depth and associated with the upper seasonal pycnocline.

The simulated turbulence field was also analyzed by evaluating the maximum dissipation rate during July (Fig. 6c). The maximum values indicate where the water column may experience short periods of intense mixing and, although these may be of short duration (related to wind events or periods during a tidal cycle, for example), they may have a significant impact on vertical transports. The maximum dissipation rates were 1–2 orders of magnitude larger than the monthly average above the shallow shelf, and an intermediate low-turbulent layer was only consistently present in a region above the shelf edge. Above the deeper areas and below the surface layer, the maximum turbulence was, in general, similar to the average conditions. A notable exception was located above the deepest part of the trench and close to the almost vertical 27.0 kg m^{-3} pycnostad (~57.8°N), where relatively high dissipation rates of ~10^{-6} W kg^{-1} were seen in a thin vertical band between 40 and 110 m depth. This narrow band with increased dissipation rates was located in the region with a large current shear between in- and out-flowing water to the Skagerrak region (Fig. 5f).

The seasonal change of vertical mixing during the growth season (March–September) was analyzed in the model at three sites located along transect 5 in the BR2018 study (shown in Fig. 1b). These sites were situated above the shallow North Sea, at the shelf-edge and above the deep channel, respectively (Fig. 7a–c). Relatively high dissipation rates of TKE in the water column were found above the shallow area with values above 10^{-7} W kg^{-1} in spring and late summer. More stratified conditions in the summer period from June–August resulted in low mid-depth turbulence ($\varepsilon \sim 10^{-8}$ W kg^{-1}) in an intermediate layer around the pycnocline. Mixing in the surface mixed layer and the benthic bottom boundary layer was high during the entire period due to meteorological forcing (e.g. wind, heat fluxes) and tidal motion above the sea bed.

Conditions at the shelf edge (Fig. 7b) during spring showed a relatively thick layer (~30–60 m) separating the surface and bottom boundary layers. This intermediate layer was characterized by low dissipation rates ($\varepsilon \sim 10^{-8}$ W kg^{-1}). A general increase of ε in the upper 50 m was seen during the summer season associated with the

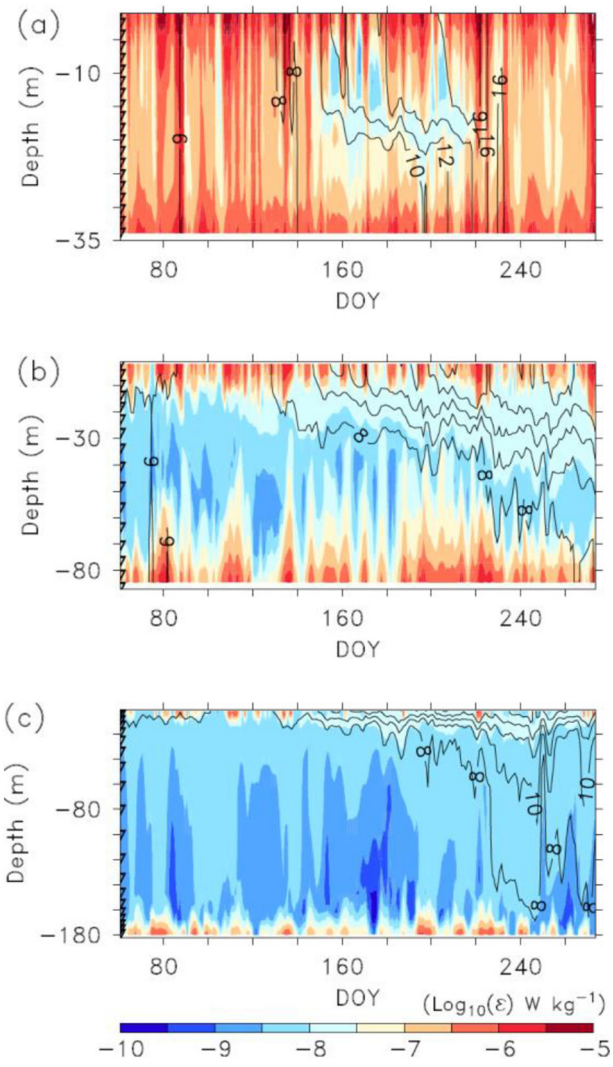

Fig. 7. Model time series from March – September (day of year, DOY) of the logarithm of the dissipation rate of TKE ($Log_{10}(\varepsilon)$, colors, W kg^{-1}) and potential temperature (contours, °C) at three locations along transect 5 (56.5°N, 57.5°N and 57.7°N, cf. Fig. 1) representing conditions (a) above the shallow shelf, (b) the shelf-edge and (c) above the Norwegian trench (note the different depth scales). Triangles along the vertical axis show the depth of the sigma-layers at the three locations in the model.

gradual deepening of the thermocline. Above the deeper parts of the channel (Fig. 7c), the separation between the surface and benthic boundary layers was also characterized by an intermediate layer exhibiting relatively low dissipation rates of TKE ($< 10^{-8}$ W kg^{-1}) during the whole period.

3.2. Nitrate assimilation above the shelf edge

The modelled average nitrate distributions in July were closely related to the distribution of water masses across the shelf edge (Fig. 8). Nitrate was depleted above the shallow shelf and in the surface layer whereas Atlantic and recirculated Atlantic water masses had a relatively high (> 1 mmol N m^{-3}) nitrate concentration. The general distribution was similar along the five transects, e.g. the 1 mmol N m^{-3} "nitrastad" became almost vertical above the shelf edge in the bottom depth range between 40 and 70 m, and further off the shelf edge the doming nitrastad was located within ~10 m from the surface.

Observations (BR2018) showed a similar distribution along transect 5 where the doming nitracline was resolved off the shelf edge and relatively high concentrations were observed in the upper 10–20 m above the Norwegian trench (Fig. 3). Observations also showed that, further off the shelf, the nitracline became deeper above the Norwegian trench and reached a minimum before the nitracline depth increased again towards the Norwegian coast (note that the observations did not include the northern area close to Norway).

The simulated nitrate concentrations off the shelf increased gradually with depth. Thus, the nitrate reservoir in the area was in the deeper water masses during this part of the year, in accordance with observations. For example, the 1 mmol N m^{-3} nitrastad was seen to almost follow the 27 kg m^{-3} pycnostad above the shelf edge. This relation to the density field indicated a dynamical relationship to the along-shelf current (Fig. 8b, d).

The *AcNA* in July was, correspondingly, closely related to the location of the 1 mmol N m^{-3} nitrastad, and the density front defined by the 27 kg m^{-3} pycnostad described the extent of nitrate assimilation above the shelf edge (Fig. 8a, c). Increased assimilation above the Norwegian trench and off the Norwegian coast was seen where the doming nitrastad approached the surface, i.e. located at ~10 m depth. The *AcNA* above the shelf edge during July was seen as an approximately 10 m deep layer at mid-depth (20–30 m) with an *AcNA* of ~2 mmol N m^{-3}. The nitrate assimilation above the Norwegian trench was 2–3 times higher and located at about 10 m depth.

An average new production was calculated for the region corresponding to the five transects visited in BR2018 from the *AcNA* in July. In general, a relatively high NP of ~100 mg C m^{-2} day^{-1} was seen above the shelf edge where the bottom depths ranged between 60 and 120 m (Fig. 9). The area with high NP increased gradually towards the Atlantic, e.g. a relatively high NP (> 100 mg C m^{-2} day^{-1}) was seen on transect 5 in a relatively broad belt off the shelf edge including areas above the Norwegian trench. The area with high NP was only ~10–20 km wide on the easternmost transect (1) and increased to ~80 km on transect 5.

3.3. Mixing by meso-scale eddies

High eddy activity was simulated in the area between the in- and outflowing water masses to the Skagerrak region and above the Norwegian trench. Meso-scale eddies were also found to influence the mixing of nitrate into the surface layer. An example is shown in Fig. 10a, where out-flowing relatively low-saline (< 31) Skagerrak water (blue color) is seen next to the shelf edge current and meanders are seen along their interface. An eddy-structure reaches from the shelf edge region and into the deeper area (along 7°E) and elevated surface nitrate concentrations were centered in the eddy (blue contour lines). The maximum concentration of nitrate in the center of the eddy was 1.6 mmol N m^{-3} and the spatial extent of the elevated nitrate concentration is ~20 km. Note that the surface concentration is close to zero (i.e. below 0.2 mmol N m^{-3}) elsewhere in the shown domain at this particular time (5 July, 23,00 h).

Thus, mesoscale eddies appear to be efficient mixing agents above the Norwegian trench. This mechanism was further analyzed by calculating the average surface nitrate concentration in July (Fig. 10b). In general, the nitrate concentration was zero or relatively small in the surface layer, except for the area above the Norwegian trench where a relatively thin belt with a significant average nitrate concentration in July of ~0.1 mmol N m^{-3} showed the influence from mixing by mesoscale eddies. The area with increased nitrate was associated with the interface between the in- and outflowing currents and was located between the 200–400 m bottom depth contours. In addition, a gradual decrease in this mixing was seen from the Atlantic towards Skagerrak. Negligible surface mixing was seen east of ~8°E.

3.4. Spatial distribution of new production

New production was analyzed along 5 transects corresponding to

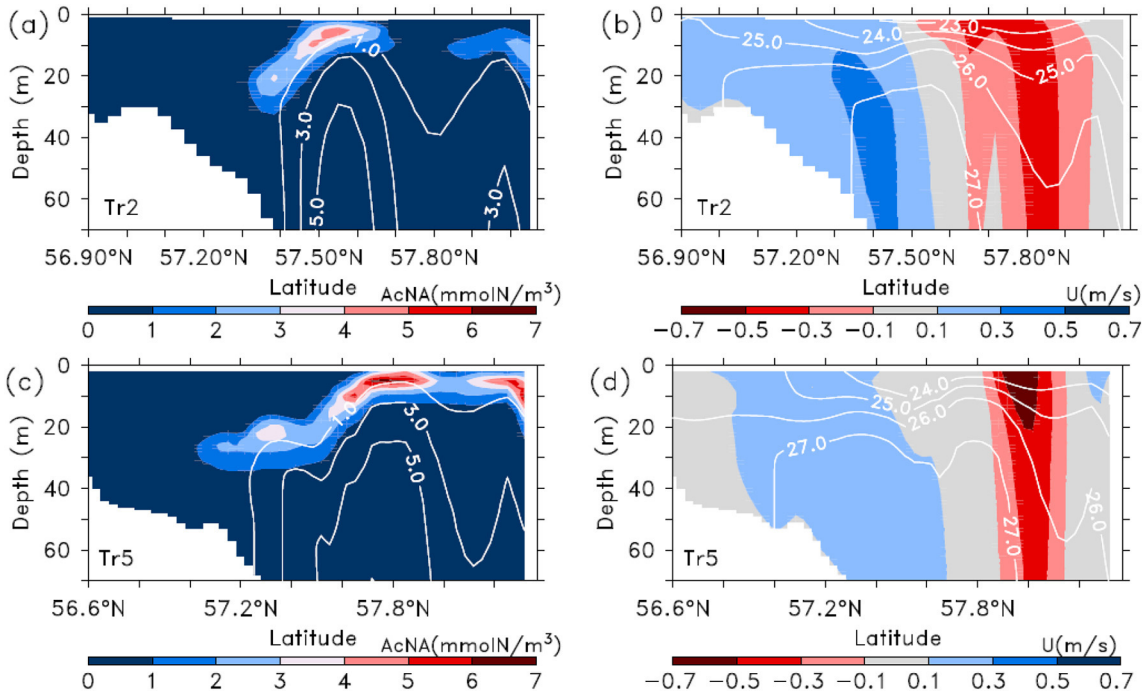

Fig. 8. Accumulated nitrate Assimilation (*AcNA*) in July along (a) transect 2 and (c) transect 5 (contours of nitrate concentration [mmol N m^{-3}]) and (b, c) corresponding monthly averaged eastward currents across the two transects (contours of potential density anomalies [kg m^{-3}]).

those visited in BR2018 (but with the extension of the transects to the Norwegian coast). The monthly averaged NP in July (Fig. 9) was calculated in four sectors: (1) the shallow shelf south of the shelf edge (bottom depth < 60 m), (2) the shelf edge (between 60 and 150 m), (3) the deep area off the shelf edge between 150 m depth and the maximum depth along the transect (i.e. above the bottom of the Norwegian trench) and (4) the area north of the trench towards Norway (Table 2). The latitude bands for the sectors were determined along each transect and the total NP was calculated in each sector (i.e. integrated NP along each line segment, in units of kg C m^{-1} day^{-1}). The area averaged NP was also calculated for each sector for comparing the spatial distribution of nitrate assimilation efficiency (i.e., in units of mg C m^{-2} day^{-1}).

The highest values of NP were found above the shelf edge along transect 5 (5.5 kg C m^{-1} day^{-1}) and above the deep area (5.4 kg C m^{-1} day^{-1}). NP above the shelf edge decreased gradually by a factor of ~5 towards transect 1. A similar decrease was seen above the deep area where the eastern transect (1) had an NP of 1.6 kg C m^{-1} day^{-1}. Some of the variation between the transects can be explained by the varying width of the shelf edge sector, e.g. the shelf edge is relatively wide at transect 4 and 5. However, the area-averaged NP also tended to decrease from transect 5 to 1 in both the shelf edge and the deep sector, with a notable exception at the shelf edge sector at transect 2 (i.e. located near the maximum curvature of the shelf where dynamics may induce increased vertical transports).

A similar trend was seen in the northern coastal sector where NP decreased from 2.8 to 1.3 kg C m^{-1} day^{-1} from transect 5 to 1. Although these values were relatively low compared with the total NP in the shelf edge and deep sectors, the area-averaged NP along the Norwegian coast was of similar magnitude (i.e., along transect 5 the coastal sector had an area-averaged NP of 108 mg C m^{-2} day^{-1} compared to 107 and 98 mg C m^{-2} day^{-1} in the shelf edge and deep sectors, respectively). Satellite images corroborate the model indication of this coastal area being a relatively productive region, as elevated chlorophyll *a* concentrations in the surface layer are frequently observed here (e.g. Fig. 1 in BR2018).

The out-flowing Skagerrak water along the Norwegian coast was found gradually to be enriched with nitrate through eddy mixing and up/downwelling along the coast. This also increased the NP as the water approached the Atlantic. Above the shallow area in the southern part of the study area, the general nitrate depletion results in a negligible NP, except along transect 5 where NP was 1.0 kg C m^{-2} day^{-1}. This was primarily taking place near the frontal zone along the shelf edge and was presumably fueled by nitrate-rich water masses at the shelf edge front.

The shelf edge and deep sector accounted for ~80% of NP in the northeastern North Sea during the model study period (~2 months) with the two sectors contributing about equally. Thus, the model results suggest that the major part of NP occurring during the period of seasonal stratification takes place via mixing at the shelf edge and in the deep sector via mixing from mesoscale eddies. The impact from mesoscale eddies is difficult to directly observe due to their transient nature (time scale ~ days) and limited spatial extent (~10–20 km). However, from observations on the VERMIX cruise, it was noted that some stations above the deep area were characterized by relatively high concentrations of chlorophyll in the SCM above the deep area and, in general, the chlorophyll concentrations at the SCM showed some horizontal heterogeneity above the Norwegian trench (BR2018). This region was generally characterized by very low vertical mixing across the nitracline. Thus, mixing from mesoscale eddies could explain the observations of relatively high chlorophyll *a* in the SCM and the primary production recorded in BR2018.

The total NP along transect 5 of 14.7 kg C m^{-1} day^{-1} decreased significantly towards the Skagerrak, i.e. a gradual decrease from transect 4 to 1 of 10.1, 7.3, 6.0 and 3.9 kg C m^{-1} day^{-1}, respectively (Table 2). This could be explained by gradual nitrate assimilation in water masses transported along the shelf edge, thus reducing the amount of nitrate being advected eastwards.

4. Discussion

The nitrate assimilation model developed here suggests considerable heterogeneity in the distribution of new production in the northeastern North Sea during the period of seasonal stratification. In some

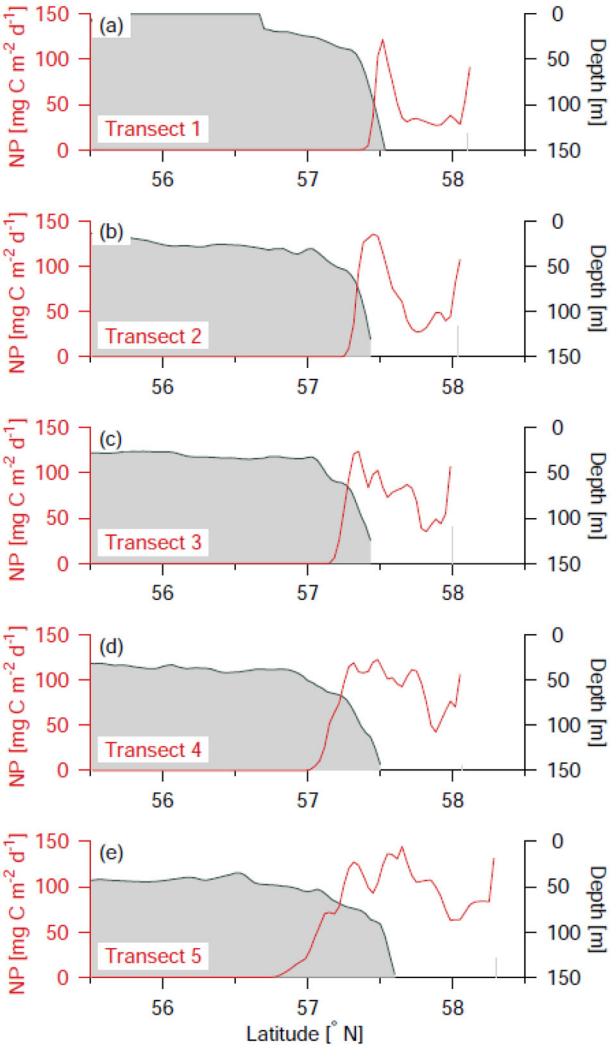

Fig. 9. Monthly averaged NP in July (red) and depth (gray shading) along transect 1–5. (For interpretation of the references to color in this figure legend, the reader is referred to the web version of this article.)

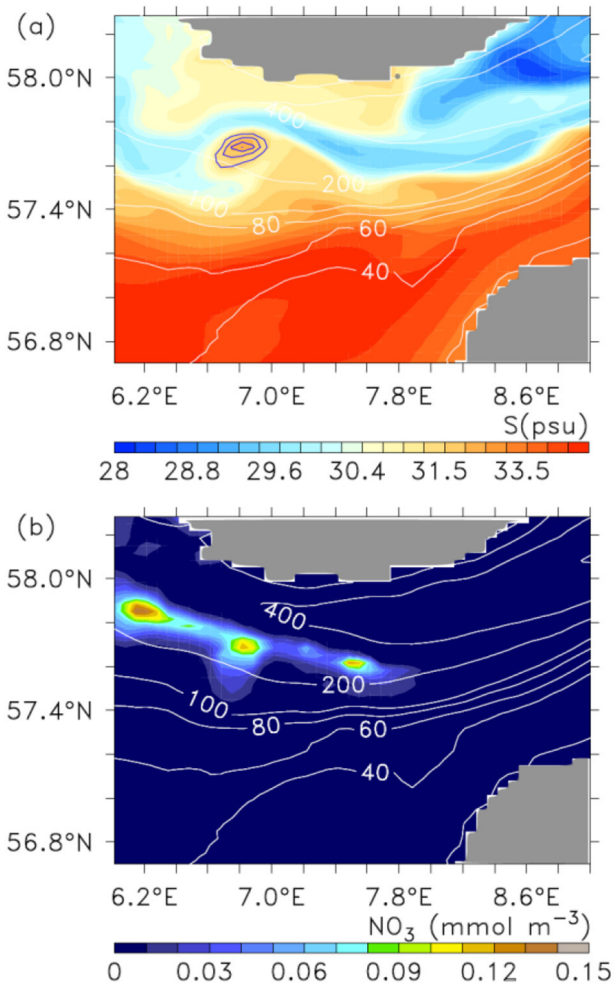

Fig. 10. (a) Surface salinity distribution from 5 July, 23:00 h (colors) and concentration of surface nitrate (blue contours, contour intervals of 0.4 mmol N m^{-3}). (b) Monthly averaged concentration of surface nitrate in July. Bathymetry is shown with white contours in (a) and (b). (For interpretation of the references to color in this figure legend, the reader is referred to the web version of this article.)

regions (a narrow belt along the shelf edge and in connection with eddy activity above the Norwegian trench) model estimates suggested a new production of up to > 100 mg C m^{-2} d^{-1}, i.e., on the same order as those estimated under spring bloom conditions (Richardson and Pedersen, 1998).

Interestingly, the region along the shelf edge where the model predicts high new production is also associated with high biodiversity (ICES, 2008) and intense fishing activity (Vespe et al., 2016). Increased fishing activity has also been observed along other parts of the northwest European shelf edge (Sharples et al., 2013). High concentrations of fish larvae have also been observed during spring in the frontal zone in the northeastern North Sea (Munk, 2014). Locations of satellite tracked harbor porpoises show that porpoises are found in higher concentrations at the shelf edge and in the deeper areas between the shelf edge and Norway in the northeastern North Sea than in surrounding waters (Sveegaard et al., 2011). High concentrations of top predators have, correspondingly, been associated with increased localized productivity in other areas of the northern North Sea (Scott et al., 2010). The presence of top-predators in the shelf-edge frontal zone and above the Norwegian trench may, therefore, be an indication of increased food availability and in accordance with the simulated distribution of new production. Thus, the processes suggested here to be important for new production in this region in the seasonally stratified North Sea may resonate through food webs in this region.

4.1. Parameterization of nitrate assimilation

The simplified nitrate assimilation model (NA-model) developed is motivated by the characteristic nutrient distributions across the shelf edge during the stratified period, i.e., nutrient depletion in the surface layer and above the shallow shelf, and high nitrate concentrations in the subsurface water masses north of the shelf edge. Similar nitrate distributions were obtained in the model simulation by initializing the model in the stratified period, and the importance of mixing from shelf edge processes and meso-scale eddies above the Norwegian trench could, thereby, be analyzed. The model is based on an assumption of a constant chlorophyll *a* concentration. This means that the spatial chlorophyll gradients established due to light, nutrients or biological processes (e.g., grazing, mortality) are not explicitly resolved. The occurrence of an SCM characterizes regions around the shelf edge and, therefore, these simplified assumptions regarding chlorophyll distribution in the model require consideration.

The NA-model assumes that chlorophyll *a* can be described by the average of the surface and SCM concentrations in the area. Thus, production at the SCM may be underestimated with the opposite being the case for surface waters. The distribution of NA (Fig. 8), however, shows

Table 2
NP in four sectors. New Production along the five transects calculated in four sectors representing the shallow shelf (bottom depth < 60 m), the shelf edge (60–150 m), the area off the shelf edge (deep) and the area towards the Norwegian coast (latitude bands define the four sectors). The total and area-averaged NP are shown for the four sectors.

Tr.	λ	φ_{60m}	φ_{150m}	φ_{deep}	NP (shallow) $\varphi \le \varphi_{60m}$		NP (shelf edge) $\varphi_{60m} < \varphi \le \varphi_{150m}$		NP (deep) $\varphi_{150m} < \varphi \le \varphi_{deep}$		NP (coastal) $\varphi > \varphi_{deep}$	
	°E	°N	°N	°N	kg C m^{-1} day^{-1}	mg C m^{-2} day^{-1}	kg C m^{-1} day^{-1}	mg C m^{-2} day^{-1}	kg C m^{-1} day^{-1}	mg C m^{-2} day^{-1}	kg C m^{-1} day^{-1}	mg C m^{-2} day^{-1}
1	8.25	57.37	57.53	57.77	0	0	1.0	53	1.6	47	1.3	40
2	7.75	57.30	57.47	57.83	0.03	0.09	1.9	105	2.6	64	1.5	59
3	7.25	57.20	57.47	57.83	0.02	0.06	2.6	89	3.0	74	1.7	75
4	6.75	57.10	57.50	57.93	0.06	0.2	4.1	93	4.2	88	1.8	99
5	6.25	57.13	57.60	58.10	1.0	2.9	5.5	107	5.4	98	2.8	108

a maximum at mid-depth in the frontal region at the shelf edge, corresponding to what would be expected from an SCM, and NA at shallow depths is shown above the Norwegian trench. This implies that NA is primarily located near the nitracline and suggests that biological consumption, in general, is more efficient in consuming nitrate at the SCM than mixing processes in transporting nitrate towards the surface layer. This is also in accordance with the observed nitrate deficient surface layer. It should also be noted that observations of chlorophyll north of the shelf edge showed relatively higher surface concentrations than observed above the shallow shelf (BR2018). This is likely due to the relatively shallow nutricline which results in the difference between surface and SCM chlorophyll concentrations being less in this area.

A sensitivity study of the NA-model to the chlorophyll concentration was conducted by simulating the June–July period with a 50% reduction of chlorophyll, i.e. $chl = 0.46$ mg chl m^{-3} (in Eq. (1), cf. Table 1). The sensitivity to the chlorophyll concentration was investigated by adding the total nitrate assimilation in July along the five transects and in the four sectors (Table 2). Nitrate assimilation in the reference case corresponded to a NP of 42.1 mg C m^{-1} day^{-1} and, in the case where the constant chlorophyll *a* concentration was reduced by 50% the nitrate assimilation was reduced to 38.3 mg C m^{-1} day^{-1}, corresponding to a 9% reduction in NP. Thus, the sensitivity of the total NP in the area to the value of *chl* in the NA-model is relatively small. This can be explained by the relatively efficient nitrate assimilation implied by Eq. (3). In other words, a reduction of chlorophyll in the model leads at first to reduced nitrate assimilation but a subsequent increase in the nitrate concentration will tend to compensate for this (Eq. (2)). Therefore, the sensitivity becomes relatively small.

Another critical aspect of the NA-model is related to the initial field and open boundary conditions of nitrate. The simulation starts from climatology in the stratified period such that the simulated nitrate field in the start of July has equilibrated with the dynamics in the model. Similarly, the open boundary conditions were simplified and the monthly climatology from June was applied during the two-month period such that variability in the region was due to local processes. This means that their impact could be identified. The resulting nitrate distributions were in accordance with observations from July.

We conclude, therefore, that the NA-model developed here is suitable for analyzing nitrate fluxes to the euphotic zone during the stratified period. Similar analyses could be carried out with more complex biological models. However, this would imply more state variables and model parameters. As these may be less well described or constrained by observations, e.g. carbon biomass, grazing rates or sinking speeds of organic matter, a more complex model might potentially introduce new uncertainties on the simulated nitrate fluxes.

The input of nitrate to the euphotic zone sets an upper limit on new production. However, if nitrate was simply removed from the euphotic zone, for example by a much simpler NA-model where nitrate concentrations were set to zero in the euphotic zone, a too strong vertical nitrate gradient would lead to an overestimate of the vertical nitrate flux and transport of nitrate in the surface layer would not be resolved. The NA-model presented here removes nitrate with a timescale dependent on photosynthesis and nitrate availability (i.e., a maximum e-folding decay-time of nitrate of ~0.8 day^{-1} near the nitracline, cf. Fig. 4) and is based on parameters representing the physiological photosynthetic processes in phytoplankton. This makes the estimate from the developed NA-model more realistic than in the simpler model.

4.2. Nitrate transport and the regional circulation

The northeastern North Sea is characterized by a relatively strong cyclonic circulation, where inflow of Atlantic water along the shelf edge recirculates in the Skagerrak with contributions from outflowing low-saline surface water from the Baltic Sea (Winther and Johannessen, 2006). The transport is estimated to be of ~1 Sv in both directions (Danielssen et al., 1990). The main influence on the area is from inflow at the northern boundary towards the Atlantic whereas the dynamics in the southern North Sea only have a minor impact (Hjøllo et al., 2009). The observed circulation pattern is in accordance with the simulated quasi-stationary circulation showing a distinct eastward current along the shelf edge current and a strong westward and low-saline outflowing current above the Norwegian trench. Other model studies also support this general circulation pattern (e.g., Pätsch et al., 2017) with an intensification of the shelf edge current towards the Skagerrak (Hordoir et al., 2008). Mixing of nitrate by mesoscale eddies was found to be an important process for sustaining NP above the Norwegian trench. Other model studies have also shown that mesoscale variability is relatively high in this region (Røed and Fossum, 2004) and eddy generation has been related to the outflowing low-saline Skagerrak water (Fossum, 2006).

Mixing processes along the shelf edge include up- or downwelling associated with wind forcing and friction against the sea bed, mixing from sub- and meso-scale eddies, tidal movements and mixing from breaking internal waves (Huthnance et al., 2009; Brink, 2016). Most of these processes are resolved explicitly in the model, e.g. the influence from wind, tides and bed friction. The generation of mesoscale eddies and their impact on the density field is known to depend on the horizontal model resolution (Lévy et al., 2010; Graham et al., 2018). Thus, the simulated nitrate assimilation above the Norwegian trench may show a similar dependence on model resolution. Mixing from breaking internal waves is an important mechanism for bringing nutrient-rich water into the euphotic zone in shelf edge regions (Sharples et al., 2007). Observations from the Celtic Sea show that breaking internal waves at the shelf edge caused significant vertical mixing (the average vertical diffusion coefficient of $\sim 10^{-4}$ m^2 s^{-1} were two orders of magnitude higher than further on the shelf) and accounted for a nitrate flux of 2 mmol N m^{-2} d^{-1} (Sharples et al., 2009). Such a nitrate flux could maintain a NP of 159 mg C m^{-2} d^{-1} (assuming a C:N of 106:16) and shows that breaking internal waves may be a significant process here. Again, these sub-grid processes (i.e., less than 2 nautical miles)

are not explicitly accounted for in the model.

Model parameterizations of vertical mixing and limitations due to the spatial resolution in the model also imply some uncertainty on the absolute values of NP. A sensitivity experiment of the significance of the constant background vertical diffusion coefficient on NP was carried out by doubling its value (i.e., to $0.2{\cdot}10^{-5}$ m^2 s^{-1}) in July and NP only increased by ~20% along the five transects compared with the reference simulation. Thus, vertical nutrient transport was mainly due to advection and vertical mixing from the k- ε turbulent scheme. The model simulation shows a general accordance with observations of water masses along the shelf edge and the general distribution of the dissipation of turbulent kinetic energy was also in good accordance with estimates from observations (BR2018) along transect 5 during a two-day period. Therefore, we argue that the simulated distribution of NP in the shelf edge region is representative for nitrate assimilation by phytoplankton in the stratified period due to the combined effect of the various mixing processes.

The simulated vertical turbulent mixing above the shallow area south of the shelf edge showed the influence from tidal mixing where the surface and benthic boundary layers tend to overlap and result in a well-mixed water column. However, at some locations, the water column becomes stratified during the summer season (e.g. Fig. 7a) such that the boundary layers are separated by a low turbulent intermediate layer. It was noted that a pronounced SCM also was observed above the shallow nitrate-depleted area during the VERMIX cruise and that the SCM was located in a similar low turbulent zone below the surface layer (BR2018). Low turbulent layers during the summer season above the otherwise well mixed shallow North Sea could potentially provide unique seasonal habitats for phytoplankton species with other traits for nitrate assimilation, e.g. diel vertical migration (e.g., Raven and Richardson, 1984), mixotrophy, or diazotrophy.

In addition to mixing of nitrate-rich subsurface water masses in the frontal area above the shelf edge and sub-mesoscale mixing above the Norwegian trench, there may be other sources of nitrate in this area. In particular, the northward nutrient transport in the Jutland coastal current from the German Bight area causes elevated nitrate concentration along the coast of Jutland and, thereby, the northeastern North Sea. These contributions are not considered in detail here although the initial nitrate distribution also contains the influence from the Jutland coastal current. However, the distribution of NP along the shelf edge is not expected to be influenced significantly by this transport, except possibly along the easternmost transect (1), because of the general cyclonic circulation in the area. In addition, nitrate sources associated with the outflowing Skagerrak water are not considered in detail and this may lead to an underestimate of NP in the coastal region adjacent to Norway. The climatological nitrate distributions show a general nitrate depletion in the surface layer during summer and, therefore, nitrate sources from the outflowing water are mostly associated with regenerated production, e.g. remineralization of dissolved organic matter, which is not considered as new production in this study. However, nitrate sources from outflow from fjords, e.g. Oslo fjord, and point sources along the coast are not included in the nitrate simulation. Therefore, the model may underestimate NP along the Norwegian coast.

5. Conclusion

New production was simulated in the northeastern North Sea during the stratified summer period by applying a new nitrate assimilation model driven by chlorophyll, light and nutrients. New production above the shelf edge was found by the model to be taking place at mid-depth (20–30 m depth) in a narrow 10–20 km wide belt, whereas the NP above the Norwegian trench was located in the upper part of the water column (~10–20 m depth) owing to the shallow nitracline in this area. New production was stimulated by mixing in the frontal zone at the shelf-edge and mixing from mesoscale eddies above the Norwegian trench. Combined, these two areas contributed with ~80% of the total NP in the area and their contributions were about equal. In general, NP decreased from the western to the eastern transect suggesting that nitrate assimilation along the shelf edge may reduce NP towards the eastern part of the North Sea. The region along the shelf edge, identified as being important for new production in the seasonally stratified North Sea, is also associated with high species richness and fishing activity as well high numbers of siting of top-predators (harbor porpoises). Thus, the new production occurring here may have important consequences for food webs in this region.

Declaration of competing interest

The authors declare that they have no known competing financial interests or personal relationships that could have appeared to influence the work reported in this paper.

Acknowledgement

This study was supported by the Danish National Science Foundation via its support of the Center for Macroecology, Evolution, and Climate (grant no. DNRF96). The Velux Foundations (grant no. 00013281) provided support for the VERMIX cruise and analysis of the measurements. The VERMIX cruise was also supported by funding for ship-time by the Danish Centre for Marine Research. The Carlsberg foundation provided support for the turbulence instrument (CF15-0301). This study has been conducted using E.U. Copernicus Marine Service Information and data from the Copernicus Data Store.

Appendix A. Supplementary data

Supplementary data to this article can be found online at https://doi.org/10.1016/j.jmarsys.2020.103414.

References

Bendtsen, J., Richardson, K., 2018. Turbulence measurements suggest high rates of new production over the shelf edge in the northeastern North Sea during summer. Biogeosciences. 15, 7315–7332. https://doi.org/10.5194/bg-15-7315-2018.

Bendtsen, J., Gustafsson, K.E., Söderkvist, J., Hansen, J.L.S., 2009. Ventilation of bottom water in the North Sea–Baltic Sea transition zone. J. Mar. Sys. 75, 138–149.

Brink, K.H., 2016. Cross-shelf exchange. Annu. Rev. Mar. Sci. 8, 59–78. https://doi.org/10.1146/annurev-marine-010814-015717.

Danielssen, D.S., Edler, L., Fonselius, S., Hernroth, L., Ostrowski, M., Svendsen, E., Talpsepp, L., 1990. Oceanographic variability in the Skagerrak and Northern Kattegat, May–June, 1990. ICES J. Mar. Sci. 54, 753–773.

Dugdale, R.C., Goering, J.J., 1967. Uptake of new and regenerated forms of nitrogen in primary productivity. Limnol. Oceanogr. 12, 196–206.

Dugdale, C., Wilkerson, F.P., 1986. The use of 15N to measure nitrogen uptake in eutrophic oceans; experimental considerations. Limnol. Oceanogr. 3, 673–689.

Egbert, G.D., Erofeeva, S.Y., 2002. Efficient inverse modeling of barotropic ocean tides. J. Atm. Ocean. Tech. 19, 183–204.

EMODnet Bathymetry Consortium, 2016. EMODnet Digital Bathymetry (DTM). https://doi.org/10.12770/c7b53704-999d-4721-b1a3-04ec60c87238.

Eppley, R.W., Peterson, B.J., 1979. Particulate organic matter flux and planktonic new production in the deep ocean. Nature 282, 677–680.

Fossum, I., 2006. Analysis of instability and mesoscale motion off southern Norway. J. Geophys. Res. 111, C08006. https://doi.org/10.1029/2005JC003228.

Garcia, H.E., Weathers, K., Paver, C.R., Smolyar, I., Boyer, T.P., Locarnini, R.A., Zweng, M.M., Mishonov, A.V., Baranova, O.K., Seidov, D., Reagan, J.R., 2018. In: Mishonov Technical, A. (Ed.), World Ocean Atlas 2018, Volume 4: Dissolved Inorganic Nutrients (Phosphate, Nitrate and Nitrate+Nitrite, Silicate). vol. 84 NOAA Atlas NESDIS (35 pp).

Graham, J.A., Rosser, J.P., O'Dea, E., Hewitt, H.T., 2018. Resolving shelf break exchange around the European northwest shelf. Geophys. Res. Lett. 45, 12.386–12.395. https://doi.org/10.1029/2018GL079399.

Hickman, A.E., Moore, C.M., Sharples, J., Lucas, M.I., Tilstone, G.H., Krivtsov, V., Holligan, P.M., 2012. Primary production and nitrate uptake within the seasonal thermocline of a stratified shelf sea. Mar. Ecol.-Prog. Ser. 463, 39–57.

Hinrichs, I., Gouretski, V., Pätsch, J., Emeis, K.-C., Stammer, D., 2017. North Sea Biogeochemical Climatology (Version 1.1). World Data Center for Climate (WDCC) at DKRZ. https://doi.org/10.1594/WDCC/NSBClim_v1.1.

Hjøllo, S.S., Skogen, M.D., Svendsen, E., 2009. Exploring currents and heat within the North Sea using a numerical model. J. Marine Sys. 78, 80–192. https://doi.org/10.

1016/j.jmarsys.2009.1006.1001.
Hordoir, R., Axell, L., Höglund, A., Dieterich, C., Fransner, F., Gröger, M., Liu, Y., Pemberton, P., Schimanke, S., Andersson, H., Ljungemyr, P., Nygren, P., Falahat, S., Nord, A., Jönsson, A., Lake, I., Döös, K., Hieronymus, M., Dietze, H., Löptien, U., Kuznetsov, I., Westerlund, A., Tuomi, L., Holt, J., Proctor, R., 2008. The seasonal circulation and volume transport on the northwest European continental shelf: a fine-resolution model study. J. Geophys. Res. 113, C06021. https://doi.org/10.1029/2006JC004034.
Hordoir, R., Axell, L., Höglund, A., Dieterich, C., Fransner, F., Gröger, M., Liu, Y., Pemberton, P., Schimanke, S., Andersson, H., Ljungemyr, P., Nygren, P., Falahat, S., Nord, A., Jönsson, A., Lake, I., Döös, K., Hieronymus, M., Dietze, H., Löptien, U., Kuznetsov, I., Westerlund, A., Tuomi, L., Haapala, J., 2019. Nemo-Nordic 1.0: a NEMO-based ocean model for the Baltic and North seas – research and operational applications. Geosci. Model Dev. 12, 363–386. https://doi.org/10.5194/gmd-12-363-2019.
Huthnance, J.M., Holt, J.T., Wakelin, S.L., 2009. Deep ocean exchange with west-European shelf seas. Ocean Sci. 5, 621–634.
ICES, 2008. Report of the ICES advisory committee 2008. In: Book 6: North Sea. International Council for the Exploration of the Sea (ICES).
Lévy, M., Klein, P., Tréguier, A.-M., Iovino, D., Madec, G., Masson, S., Takahashi, K., 2010. Modifications of gyre circulation by sub-mesoscxale physics. Ocean Modell 34, 1–15. https://doi.org/10.1016/j.ocemod.2010.04.001.
Luyten, P. (Ed.), 2014. COHERENS—A Coupled Hydrodynamical- Ecological Model for Regional and Shelf Seas: User Documentation. Version 2.6. RBINS Report. Operational Directorate Natural Environment, Royal Belgian Institute of Natural Sciences.
Munk, P., 2014. Fish larvae at fronts: horizontal and vertical distribution of gadoid fish larvae across a frontal zone at the Norwegian Trench. Deep Sea-Res. II 107, 3–14.
O'Dea, E.J., Arnold, A.K., Edwards, K.P., Furner, R., Hyder, P., Martin, M.J., Siddorn, J.R., Storkey, D., While, J., Holt, J.T., Liu, H., 2012. An operational ocean forecast system incorporating NEMO and SST data assimilation for the tidally driven European North-West shelf. J. Operational Oceanogr. 5, 3–17.
Pätsch, J., Burchard, H., Dieterich, C., Gräwe, U., Gröger, M., Mathis, M., Kapitza, H., Bersch, M., Moll, A., Pohlmann, T., Su, J., Ho-Hagemann, Ha T.M., Schulz, A., Elizalde, A., Eden, C., 2017. An evaluation of the North Sea circulation in global and regional models relevant for ecosystem simulations. Ocean Model 116, 70–95.
Platt, T., Gallegos, C.L., Harrison, W.G., 1980. Photoinhibation of photosynthesis in natural assemblages of marine phytoplankton. J. Mar. Res. 38, 687–701.
Raven, J.A., Richardson, K., 1984. Dinophyte flagella: a cost-benefit analysis. New Phytol. 98, 259–276.
Redfield, A.C., Ketchum, B.H., Richards, F.A., 1963. The influence of organisms on the composition of sea water. In: Hill, M.N. (Ed.), The Sea. Wiley-Interscience, New York, pp. 26–77.
Richardson, K., Bendtsen, J., 2017. Photosynthetic oxygen production in a warmer ocean: the Sargasso Sea as a case study. Phil. Trans. R. Soc. A, 20160329. https://doi.org/10.1098/rsta.2016.0329.
Richardson, K., Pedersen, F.B., 1998. Estimation of new production in the North Sea: consequences for temporal and spatial variability of phytoplankton. ICES J. Mar. Sci. 55, 574–580.
Richardson, K., Bendtsen, J., Kragh, T., Mousing, E.A., 2016. Constraining the distribution of photosynthetic parameters in the global ocean. Front. Mar. Sci. 3, 269. https://doi.org/10.3389/fmars.2016.00269.
Røed, L.P., Fossum, I., 2004. Mean and eddy motion in the Skagerrak/northern North Sea: insight from a numerical model. Ocean Dynam. 54, 197–220. https://doi.org/10.1007/s10236-003-0076-1.
Scott, B.E., Sharples, J., Ross, O.N., Wang, J., Pierce, G.J., Camphuysen, C.J., 2010. Sub-surface hotspots in shallow seas: fine-scale limited locations of top predator foraging habitat indicated by tidal mixing and sub-surface chlorophyll. Mar. Ecol. Prog. Ser. 408, 207–226. https://doi.org/10.3354/meps08552.
Sharples, J., Moore, C.M., Rippeth, T.P., Holligan, P.M., Hydes, D.J., Fisher, N.R., Simpson, J.H., 2001. Phytoplankton distribution and survival in the thermocline. Limnol. Oceanogr. 46, 486–496.
Sharples, J., Tweddle, J.F., Green, J.A.M., Palmer, M.R., Kim, Y.-N., Hickman, A.E., Holligan, P.M., Moore, C.M., Rippeth, T.P., Simpson, J.H., Krivtsov, V., 2007. Spring-neap modulation o internal tide mixing and vertical nitrate fluxes at a shelf edge in summer. Limnol. Oceanogr. 52, 1735–1747.
Sharples, J., Moore, C.M., Hickman, A.E., Holligan, P.M., Tweddle, J.F., Palmer, M.R., Simpson, J.H., 2009. Internal tidal mixing as a control on continental margin ecosystems. Geophys. Res. Lett. 36, L23603. https://doi.org/10.1029/2009GL040683.
Sharples, J., Ellis, J.R., Nolan, G., Scott, B.E., 2013. Fishing and the oceanography of a stratified shelf sea. Progr. Oceanography 117, 130–139. https://doi.org/10.1016/j.pocean.2013.06.014.
Shchepetkin, A.F., McWilliams, J.C., 2003. A method for computing the horizontal pressure gradient force in an oceanic model with a nonaligned vertical coordinate. J. Geophys. Res. 108 (C3), 3090. https://doi.org/10.1029/2001JC1047.
Siddorn, J.R., Furner, R., 2013. An analytical stretching function that combines the best attributes of geopotential and terrain-following vertical coordinates. Ocean Model 66, 1–13. https://doi.org/10.1016/j.ocemod.2013.02.001.
Song, Y., Haidvogel, D.B., 1994. A semi-implicit ocean circulation model using a generalized topography-following coordinate system. J. Comp. Phys. 115, 228–244.
Sveegaard, S., Teilmann, J., Toutgaard, J., Dietz, R., Mouritsen, K.N., Desportes, G., Siegert, U., 2011. High-density areas for harbor porpoises (*Phocoena phocoena*) identified by satellite tracking. Mar. Mamm. Sci. 27, 230–246. https://doi.org/10.1111/j.1748-7692.2010.00379.x.
Vespe, M., Gibin, M., Alessandrini, A., Natale, F., Mazzarella, F., Osio, G.C., 2016. Mapping EU fishing activities using ship tracking data. J. Maps. 12 (sup1), 520–525. https://doi.org/10.1080/17445647.2016.1195299.
Volk, T., Hoffert, M.I., 1985. Ocean carbon pumps: Analysis of relative strengths and efficiencies in ocean-driven atmospheric CO_2. In: Sundquist, E.T., Broecker, W.S. (Eds.), The Carbon Cycle and Atmospheric CO_2: Natural Variations Archean to Present, Geophysical Monograph Series. vol. 32. AGU, Washington, DC, pp. 99–110.
Weston, K., Fernand, L., Mills, D.K., Delahunty, R., Brown, J., 2005. Primary production in the deep chlorophyll maximum of the central North Sea. J. Plankton Res. 27, 909–922.
Winther, N.G., Johannessen, J.A., 2006. North Sea circulation: Atlantic inflow and its destination. J. Geophys. Res. 111, C12018. https://doi.org/10.1029/2005JC003310.